CO_2 adsorption on *Miscanthus×giganteus* (MG) chars prepared in different atmospheres

Hong Tian[1], Tong Zhou[1], Jiawei Wang[2], Filipe Rego[2], Yang Yang[2], Huan Xiang[2], Yanshan Yin[1], Wei Liu[1], Anthony V. Bridgwater[2]

[1] *School of Energy & Power Engineering, Changsha University of Science & Technology, Changsha 410114, China*

[2] *Bioenergy Research Group, EBRI, Aston University, Birmingham B4 7ET, UK.*

ABSTRACT

Low-cost solid sorbents with enhanced capacity and selectivity towards CO_2 are crucial in the design of an efficient carbon capture process. The suitability of chars prepared by the slow pyrolysis of *Miscanthus×giganteus* (MG) in different atmospheres as CO_2 adsorbents was explored. The adsorption performance of the MG chars was evaluated using a thermogravimetric analyser. The results showed that the CO_2 uptakes at 30 °C were between 1.528 to 1.811 mmol·g^{-1} for chars prepared in N_2, between 0.208 to 1.746 mmol·g^{-1} for chars prepared in CO_2, and between 1.483 to 1.774 mmol·g^{-1} for chars prepared in He, respectively. These values were in line with those from the literature on biomass-derived carbon-based materials. The cyclic adsorption/desorption regeneration experiments showed that 180 °C was the best temperature for CO_2 desorption from the MG chars. The char prepared at 800 °C in nitrogen exhibited the best regeneration performance, i.e. losing 13.86% of its adsorption capacity after seven adsorption/desorption cycles. These results suggested that the biomass waste used in this work could be successfully valorised as efficient CO_2 adsorbents with excellent cyclic performance.

Keywords: *Miscanthus×giganteus* char, Different atmospheres, CO_2 capture, Low-cost adsorbents, Cyclic adsorption/desorption measurement

1. Introduction

Due to the continuously growing energy demands, it is expected that fossil fuels will continue to play a vital role in energy generation and many other industrial processes despite the deployment of alternative technologies [1]. Excessive emissions of CO_2 and other greenhouse gases (GHGs) from fossil fuel consumption have caused severe global warming and climate change [2-4]. In the last two decades, carbon capture, storage and utilisation (CCSU) has been recognised as one of the key technologies to deliver a low carbon utilisation of fossil fuels and reach the target of CO_2 emission reduction.

Among all carbon capture technologies, the capture of CO_2 using solid adsorbents has the advantages of high operation flexibility and low maintenance cost [5]. So far, a variety of adsorbents have been studied for capturing CO_2 from flue gas, including zeolites [6], metal-organic frameworks (MOFs) [7], polymers of intrinsic microporosity (PIMs) [8, 9], hyper-cross-linked polymers (HCPs) [10, 11], conjugated microporous polymers (CMPs) [12, 13], amine-modified mesoporous silica [14], calcium oxide [15, 16] and carbon-based materials. Compared to other solid

adsorbents, carbon-based materials display a relatively high CO_2 adsorption capacity and selectivity under a wide range of operating conditions due to their high specific surface area, well-defined porosities, larger pore volume and adjustable surface properties [17-19].

Chars derived from biomass have been investigated as energy materials for a long time due to their renewable and carbon-neutral nature. Moreover, apart from its energy content, chars also have suitable porous structures and unique surface properties for efficient CO_2 adsorption. Chars and the derived activated carbons (ACs) from different biomass were studied for CO_2 capture [19-22]. The results showed that the final product's physic-chemical properties depended on the nature of the biomass feedstock, carbonisation conditions, activation agents, and activation conditions [22].

It has been demonstrated that the properties of the feedstock could obviously affect the CO_2 adsorption capacity of chars produced. Shahkarami et al. [22] investigated the CO_2 adsorption capacity of the ACs derived from different waste biomass. The breakthrough adsorption capacities of the ACs derived from wheat straw, flax straw, sawdust, willow ring and poultry litter were 1.498, 1.511, 1.384, 1.602, and 1.593 $mmol \cdot g^{-1}$, respectively. This work demonstrated that the adsorption capacity of ACs and selective adsorption of CO_2, O_2 and N_2 by ACs could be controlled and optimised through the choice of raw materials and carbonisation conditions (fast and slow pyrolysis under 500 ^oC). Creamer et al. [23] pyrolysed bagasse and hickory wood under N_2 atmosphere at 600 ^oC, and carried out CO_2 adsorption experiments on the obtained chars. The CO_2 adsorption capacities of bagasse char and hickory wood char were 1.67 and 1.39 $mmol \cdot g^{-1}$ at 25 ^oC and 1 atm, respectively. Plaza et al. [24] found that the CO_2 adsorption capacities of the chars produced from the olive core and almond shell (treated under same conditions) were 0.75 and 0.7 $mmol \cdot g^{-1}$, respectively. Therefore, even under similar char preparation conditions, the CO_2 adsorption capacity of the chars from different feedstock could be considerably different.

The yield, pore structure and surface chemical properties of biomass-derived char are also affected by char production temperature. With increasing char production temperature, the ratio of hydrogen to oxygen in the produced char decreased, while the degree of aromaticity and specific surface area increased, leading to higher adsorption capacity. The research by Creamer et al. [23] showed that the bagasse char produced at 600 °C had the highest CO_2 adsorption capacity of 1.672 $mmol \cdot g^{-1}$ at 25 °C, while the char produced at 300 °C could only capture 0.795 $mmol \cdot g^{-1}$ CO_2 at 25 °C. Madzaki [24] vaporised sawdust in a lab-scale air blown gasifier reactor at 450, 750 and 850 °C, respectively, and the CO_2 adsorption capacities of the produced chars were 0.45, 1.03 and 1.08 $mmol \cdot g^{-1}$ at 30 °C and 1 atm, respectively. Huang et al. [25] measured the CO_2 adsorption capacity of the chars from rice straw heated at 250–600 °C in an anoxic circumstance. The CO_2 adsorption capacity (at 30 ^oC and 1atm) of the chars increased with char production temperature. The adsorption capacity of the char prepared at 250 °C was only about 0.295 $mmol \cdot g^{-1}$, whereas the char prepared at 550 °C showed an enhanced capacity of 1.136 $mmol \cdot g^{-1}$.

Char production atmosphere is another important parameter affecting char's physical and chemical properties, hence their CO_2 adsorption capacity. Zhuo et al. [26] prepared carbon cellulose aerogels by a two-step carbonization-activation method in different atmospheres. The CO_2 adsorption capacities of the carbon cellulose aerogels prepared in N_2 and CO_2 were 3.00 and 3.42 $mmol \cdot g^{-1}$ at 25 ^oC and 1atm, respectively. Valentina et al. [19] and Heo et al. [27] carbonised the cellulose fibre in an steam atmosphere and N_2 atmosphere at 700 ^oC, respectively. The CO_2 adsorption capacities of the derived chars were 2.33 and 2.21 $mmol \cdot g^{-1}$ at 25 ^oC and 1 atm, respectively. Additionally, even in

the same atmosphere, different gas concentrations can lead to a difference in the CO_2 adsorption capacity of chars prepared. Plaza et al. [28] prepared carbon adsorbents using almond shell and olive stone as raw materials in an oxygen atmosphere (3%–5% of oxygen) at 650 °C. The results showed that the CO_2 adsorption capacities of almond shell char and olive stone char were 1.92–2.02 and 1.90–2.11 $mmol \cdot g^{-1}$ at 25 °C and 1atm with an oxygen concentration of 3%, and they were 1.78–1.98 and 1.90–2.09 $mmol \cdot g^{-1}$ with an oxygen concentration of 5% at 25 °C and 1atm, respectively.

Physical/chemical activation method also has a significant effect on the CO_2 adsorption capacity of chars. The CO_2 adsorption uptake of the AC activated by KOH was 7.14 $mmol \cdot g^{-1}$ at 1 bar and 0 °C, which was much higher than that of the AC (2.78 $mmol \cdot g^{-1}$) prepared by direct activation of corn straw [29]. Manya et al. [30] prepared ACs from grapevine char by physical activation and chemical activation of CO_2 and KOH, respectively. Their CO_2 adsorption capacities were 3.1 and 4 $mmol \cdot g^{-1}$ at 25 °C and 1 atm, respectively. A series of porous carbon materials were developed for CO_2 capture by simple carbonisation and KOH activation of coconut shells under very mild conditions [20]. Owing to the high amount of narrow micropores within the carbon framework, the porous carbon prepared at a KOH/precursor ratio of 3 and 600 °C exhibited an enhanced CO_2 adsorption capacity of 4.23 and 6.04 $mmol \cdot g^{-1}$ at 25 and 0 °C under 1 bar, respectively. Plaza [31] studied carbons prepared from biomass by two methods, i.e. physical activation with CO_2 and amination. The results showed that activated samples showed faster adsorption kinetics, which is due to the presence of transport pores that is the transport channel of gas adsorption by biomass char. In addition, aminated samples had narrower porosities but higher volumetric capacities compared to physical activation with CO_2. It can conclude that both activation methods and agents have a significant impact on the CO_2 adsorption capacity of the products. Regarding the structural properties of char/ACs, Valentina et al. [19, 32, 33] showed that micropores (pore size < 0.7 nm) played a crucial role in the process of CO_2 adsorption.

Miscanthus×giganteus (MG) is a widely distributed C4 perennial rhizome herb, mainly composed of cellulose, hemicellulose and lignin. It is considered to be one of the most potential high-yield fibre energy plants. MG is native to the subtropical and tropical regions of Africa and Asia and can grow well in various climates [34]. Its economic benefit is believed to be higher than other energy plants, such as sorghum or poplar, due to the very high growth rate, high biological weight, low plantation cost, high calorific value, and low ash content [34]. It is, therefore, essential to develop the efficient utilisation of MG for optimising its energy application.

Despite the wide investigation of MG's bioenergy potential, there is no report on the possibility of MG derived chars in CO_2 capture application. In this study, a series of chars with different characteristics were prepared from MG in three typical atmospheres, i.e. carbon dioxide (CO_2), nitrogen (N_2) and helium (He), at 600, 800 and 1000 °C respectively. The physic-chemical properties of different chars were studied, and their adsorption capacity of CO_2 was measured by the thermogravimetric analyser. The regeneration performance of char was measured by adsorption/desorption cycles.

2. Materials and methods

2.1. Feedstocks preparation

The feedstock MG was obtained from Changsha, China (Hunan Agriculture University, China). MG samples were firstly milled and then sieved to fine particles of less than 74 μm. The samples were then stored at ambient conditions in sealed bags.

2.2. Char preparation and characterisation

The ground MG samples were pyrolysed using different carrier gases (N_2, He and CO_2) and char production temperatures (600, 800, and 1000 °C) in a vacuum tube furnace (SK-1600, Tianjin, China). Approximately 2 g of sample was placed in the furnace for each run. High purity carrier gas (50 mL·min^{-1}) was used to purge the furnace for 30 minutes to eliminate the air in the system before heating. After that, the furnace temperature was increased from room temperature to the char production temperature at a constant heating rate of 10 °C·min^{-1}. The oxygen-free atmosphere was created by the continuous flow of the carrier gas. The final temperature was maintained for 1 h to ensure complete conversion. After each pyrolysis run, the cooled MG chars were collected, weighed and stored in sealed sample bags for further experiments. The MG chars obtained with the carrier gases of N_2, He, and CO_2 were named as N_2-*TJ*, He-*TJ*, and CO_2-*TJ*, respectively, where *T* refered to the char production temperature used in the pyrolysis process.

The pore structure of the chars were characterized by N_2 adsorption at 77 K using Micromeritics ASAP 2020 nitrogen adsorption instrument. Specific surface areas were determined by the Brunauer-Emmett-Teller (BET) model, the pore sizes distribution was presented following the Barrett-Johner-Halenda (BJH) model. The chemical functional groups of the chars were analyzed using a Nicolet IS10 FTIR Spectrometer in the range of 4000-400 cm^{-1}, and 32 scans were taken at a resolution of 4 cm^{-1}.

The detailed characterisation of the chars was reported in our previous work using scanning electron microscope-energy dispersive X-ray spectroscopy (SEM-EDX), Brunauer-Emmett-Teller (BET) N_2 adsorption, X-ray diffraction (XRD) [35]. The SEM analysis of MG char showed that with char preparation temperature increased from 600 to 1000 °C, N_2 char structure further fractured with more cracks appeared. Many pores appeared on the He char surface at 800 °C, while slight deformation and melting phenomenon were observed at 1000 °C. For CO_2 char, high preparation temperature caused surface cracking deepened, with increased surface pores and roughness leading to collapses on the material surface. Furthermore, the increase of MG char preparation temperature could increase the relative contents of Ca, Mg and K in the CO_2 char but reduce the contents of Ca and K in the N_2 char by EDX characterisation. The trends of Ca, Mg and K content in the He char first increased and then decreased with the increase of preparation temperature. The BET analysis of MG char presented that with the MG char preparation temperature increased from 600 to 1000 °C, the S_{BET} of N_2 char and He char increased. For CO_2 char, the S_{BET} first increased from 600 to 800 °C but eventually vanished due to the neck formation and melting phenomenon of CO_2-1000. The XRD analysis showed that high preparation temperature enhanced the degree of aromatisation in carbon structures for N_2 char and He char. The structure of CO_2 char was becoming more graphitic at high preparation temperature.

2.3. CO_2 adsorption measurements

CO_2 adsorption was measured by a Netzsch TGA 449 F3 thermogravimetric analyser. Approximately 10 mg of each sample was heated from ambient temperature to 105 °C at 20 °C·min^{-1} in N_2 atmosphere. The sample was held at 105 °C for 30 min and then cooled to 30 °C, and it was held at 30 °C for 10 min. The gas input was switched from N_2 to CO_2 and held isothermally for 90 min. It was found that the mass fluctuated within 3% after more than an hour in the study. The CO_2 adsorption capacity was determined from the weight change in CO_2. The effects of the change in gas viscosity and gas density were corrected by measuring the response to an empty platinum crucible by the same

method. To investigate the recyclability of the porous carbon in CO_2 capture, the used adsorbent was evacuated by degassing at 140 °C for 10 min in N_2 atmosphere [36]. The CO_2 adsorption isotherm of the regenerated adsorbent was then recorded at 30 °C. This procedure was repeated eight times to confirm long term stability and reusability.

3. Results and discussion

3.1. CO_2 adsorption experiment

The TGA curves of CO_2 adsorption capacity measurement are shown in Fig. 1. The CO_2 adsorption analysis included three stages. In the first stage, the MG char was pretreated at 105 °C for 30 minutes in an N_2 atmosphere. The weight loss was caused by the release of adsorbed water at this stage. Then, the MG char was cooled to the adsorption temperature (30 °C) in the second stage, and the adsorption of N_2 on the MG char caused a slight weight increase. After the temperature of the MG char was stable at 30 °C, the input gas was switched from N_2 to CO_2 in the third stage. The weight increase in this stage was due to the CO_2 adsorption.

Table 1 Structural parameters of N_2 adsorption of MG chars at 77 K.

Samples	S_{BET} ($m^2 \cdot g$)	S_{micro} ($m^2 \cdot g^{-1}$)	V_{total} ($cm^3 \cdot g^{-1}$)	V_{micro} ($cm^3 \cdot g^{-1}$)	V_{meso} ($cm^3 \cdot g^{-1}$)	V_{micro}/V_{total}	Mean pore size (nm)
N_2-600J	403.46	259.82	0.2163	0.1876	0.0287	0.8673	2.1442
N_2-800J	629.32	476.74	0.3666	0.2895	0.0771	0.7897	2.3300
N_2-1000J	981.75	788.17	0.5665	0.3350	0.2315	0.5914	2.3082
He-600J	214.69	140.41	0.1607	0.0890	0.0717	0.5538	2.9944
He-800J	495.38	325.05	0.2867	0.2456	0.0411	0.8566	2.3152
He-1000J	809.01	698.40	0.4266	0.2760	0.1560	0.6470	2.1090
CO_2-600J	467.09	313.52	0.2629	0.2070	0.0559	0.7874	2.2512
CO_2-800J	632.15	419.73	0.2727	0.2446	0.0281	0. 8960	1.7257
CO_2-1000J	1.1810	0.756	0.0033	0.0030	0.0003	0.9091	57.391

As we all know, the structural characteristics and surface chemistry of adsorbents have a great influence on their CO_2 adsorption capacity. For carbon-based adsorbents, the main parameters controlling the adsorption capacity and selectivity of carbon dioxide at low partial pressure and ambient temperature were micropores, such as volume and pore size, and surface functionalisation of pores. Narrow micropores were favourable for adsorption. The gas adsorption depended on short-term non-specific interaction between gas and adsorbent. In contrast, at higher pressures, surface coverage became the main factor, so wider pores determined the gas adsorption [37]. As shown in Fig. 2, when the char production temperature rose from 600 °C to 1000 °C, the CO_2 adsorption capacity of MG chars at 30 °C (except for CO_2-1000J) increased, i.e. from 1.628 $mmol \cdot g^{-1}$ to 1.811 $mmol \cdot g^{-1}$ under N_2 atmosphere, from 1.483 $mmol \cdot g^{-1}$ to 1.774 $mmol \cdot g^{-1}$ under He atmosphere, and from 1.524 $mmol \cdot g^{-1}$ at 600 °C to 1.746 $mmol \cdot g^{-1}$ at 800 °C under CO_2 atmosphere. The reason of the adsorption capacity of CO_2-1000J dropped to 0.208 $mmol \cdot g^{-1}$ at 1000 °C was that the char structure was further fractured with more and more cracks and the carbon skeleton was destroyed. In addition, char directly reacted with CO_2 at high temperature through the Boudouard reaction ($CO_2+C \rightarrow 2CO$) and caused elimination of carbon links, leading to the phenomenon of sintering and fragmentation. The CO_2-1000J contains almost ash (76.95%), meaning the lack of enough carbon to maintain the porous framework

[35].The enhanced porosity of MG chars can improve the adsorption capture of CO_2. Table 1 shows that the porosity of MG chars was enhanced due to high temperature (except for CO_2-1000J), such as S_{BET}, V_{total}, and V_{micro}. The order of S_{BET}, V_{total}, and V_{micro} sequence for MG char under the same MG char preparation temperature (600 and 800 °C) can be ranked as CO_2 char > N_2 char > He char. It is because CO_2 is the activating agent to create high S_{BET}, V_{total}, and V_{micro} under activation process. The reason of high S_{BET} (except for CO_2-1000J) is that MG samples are milled and then sieved to fine particles of less than 74 μm before experiments. The specific surface area and pore structure play a key role in CO_2 capturing capacity [38, 39]. It was observed that the adsorption-desorption isotherms of MG chars had H4 type hysteresis loops, which was associated with the samples with narrow slit-like pores, and the MG chars contained a large number of micropores less than 1 nm [35]. The slit-like pores and the microporous structures could significantly improve the CO_2 adsorption capacity of MG chars [16, 19, 32, 40].

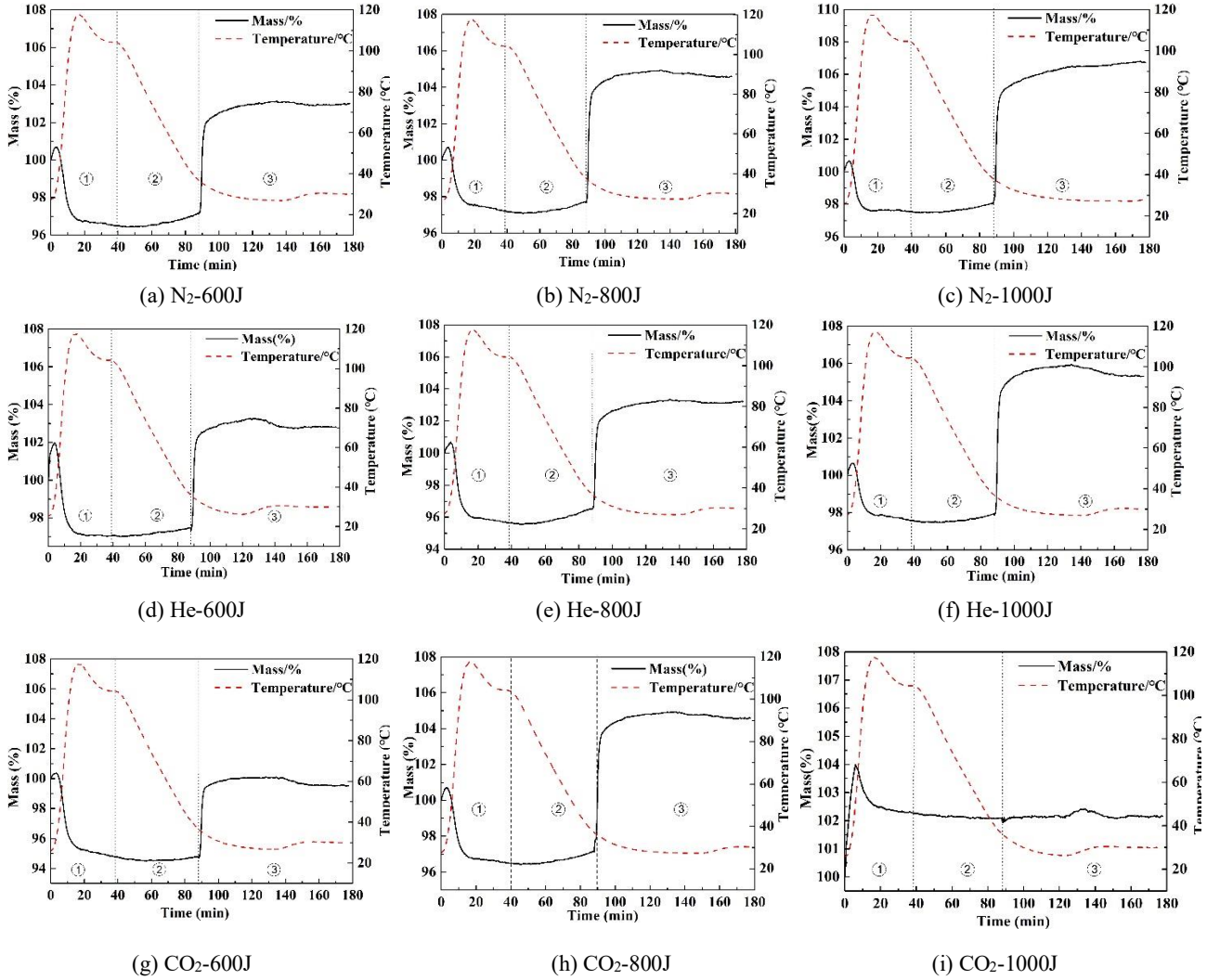

(a) N_2-600J (b) N_2-800J (c) N_2-1000J

(d) He-600J (e) He-800J (f) He-1000J

(g) CO_2-600J (h) CO_2-800J (i) CO_2-1000J

Fig. 1 CO_2 adsorption curves of MG chars: (a)-(c) N_2 atmosphere, (d)-(f) He atmosphere and (g)-(i) CO_2 atmosphere.

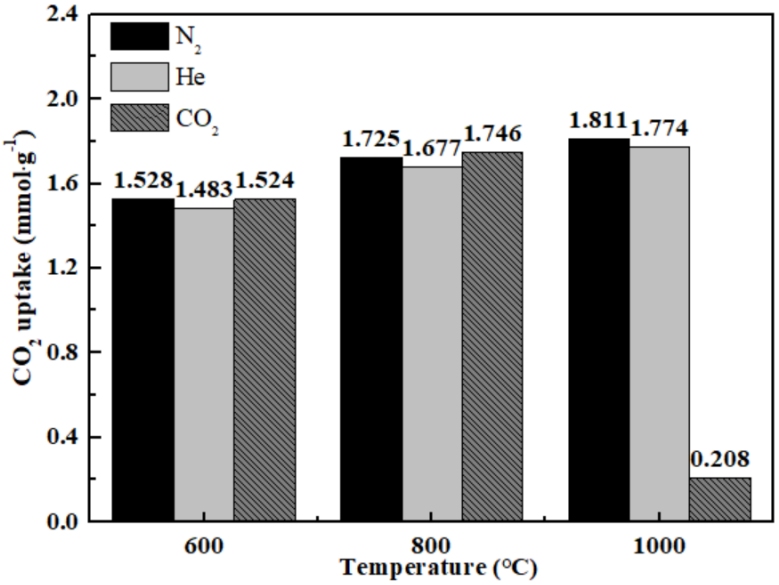

Fig. 2 CO_2 adsorption capacity of MG chars prepared under different atmospheres and temperatures.

189

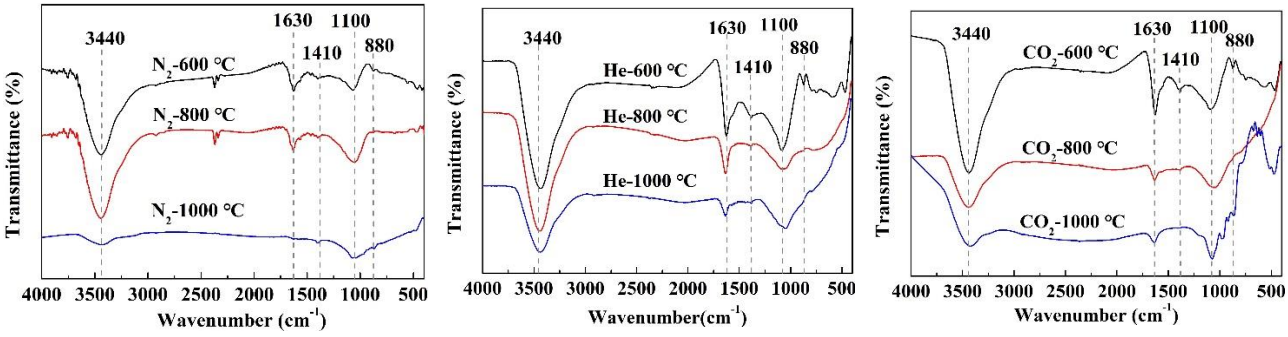

(a) N_2 (b) He (c) CO_2

190 Fig. 3 FTIR spectrum of MG char samples under different atmosphere: (a) N_2 atmosphere, (b) He atmosphere and (c) CO_2 atmosphere.

191

192 Fig. 3 shows the FTIR analysis on the surface functional groups of char samples under different atmospheres.
193 The hydroxyl peak at 3440 cm^{-1} attributed to the $-OH$ stretching vibration of alcohols, phenols, and carboxylic
194 acids in chars. Meanwhile, the one centered at 1630 cm^{-1} came from the conjugated C=C stretching vibration. The
195 peak at 1410 cm^{-1} was assigned to the fatty chain CH_3-, CH_2-. The peak at 1300 cm^{-1} was the characteristic of the
196 $-NH_2$ vibration. The peak at 1100 cm^{-1} was attributed to the aromatic ring tensile vibration or C−O tensile vibration.
197 The C−H vibration of the aromatic nucleus was centered at 880 cm^{-1}. The different char production atmospheres
198 also affect the porous structures of the MG chars and their CO_2 adsorption capacity. The N_2 adsorption data showed
199 that the S_{BET}, V_{total}, and V_{micro} of He-600J and He-800J were significantly lower than those of N_2-J and CO_2-J prepared
200 at the same temperature, but the difference in CO_2 adsorption capacity was small. The main reason was that inert gas
201 He has a strong protective effect, resulting in the surface of He-J chars were rich in hydroxyl, amino and other
202 functional groups, which could improve their adsorption capacity through chemical adsorption [41-44].

203 **3.2 Recyclability experiment**

204 Table 2 CO_2 adsorption capacity ($mmol \cdot g^{-1}$) at 30 °C and adsorption loss rate of MG char cyclic desorption at 140 °C.

Samples	Cycles								1-Loss [a] (%)	4-Loss [b] (%)	7-Loss [c] (%)
	1	2	3	4	5	6	7	8			
N_2-600J	1.528	1.323	1.259	1.152	1.093	1.081	1.069	1.063	13.42	24.61	30.43
N_2-800J	1.725	1.641	1.555	1.498	1.452	1.424	1.408	1.405	4.87	15.83	22.78
N_2-1000J	1.811	1.567	1.498	1.437	1.393	1.376	1.372	1.352	13.47	23.08	33.94
He-600J	1.483	1.293	1.187	1.074	1.042	1.023	1.021	0.993	12.81	27.58	33.04
He -800J	1.677	1.383	1.294	1.261	1.245	1.244	1.229	1.203	17.53	24.81	28.26
He -1000J	1.783	1.601	1.541	1.509	1.418	1.378	1.387	1.342	10.21	15.36	24.73
CO_2-600J	1.524	1.309	1.189	1.157	1.087	1.059	1.064	1.027	14.11	24.08	32.31
CO_2-800J	1.746	1.533	1.477	1.403	1.366	1.366	1.362	1.345	12.20	19.64	22.97
CO_2-1000J	0.208	0.161	0.168	0.152	0.082	0.084	0.082	0.052	22.60	26.92	75.00

[a] Adsorption loss rate of MG after desorption for one time. [b] Adsorption loss rate of MG after desorption for four times. [c] Adsorption loss rate of MG after desorption for seven times.

To understand the CO_2 adsorption process on MG chars, it was not only necessary to determine the optimal char production atmosphere/temperature but also to investigate the effect of high-temperature desorption on the cyclic regeneration of the products. Ideal CO_2 adsorbents should easily be regenerated and maintain their adsorption performance. To evaluate the CO_2 adsorption performance of MG chars after multiple cycles of CO_2 adsorption, a series of continuous adsorption-regeneration cycle experiments were carried out. Each experiment includes the following steps: pretreatment at 105 °C for 30 min in N_2 atmosphere, adsorption at 30 °C for 10 min in CO_2 atmosphere, and desorption at 140 °C for 10 min in N_2 atmosphere [45]. Fig. 4 shows the CO_2 adsorption capacity and cyclic regeneration of MG chars. For each group of MG chars prepared under different atmospheres at different char production temperatures, a total of seven adsorption/desorption cycles were carried out. The actual CO_2 adsorption capacity of the MG char was calculated by the mass difference of adsorption/desorption. The results are shown in Table 2.

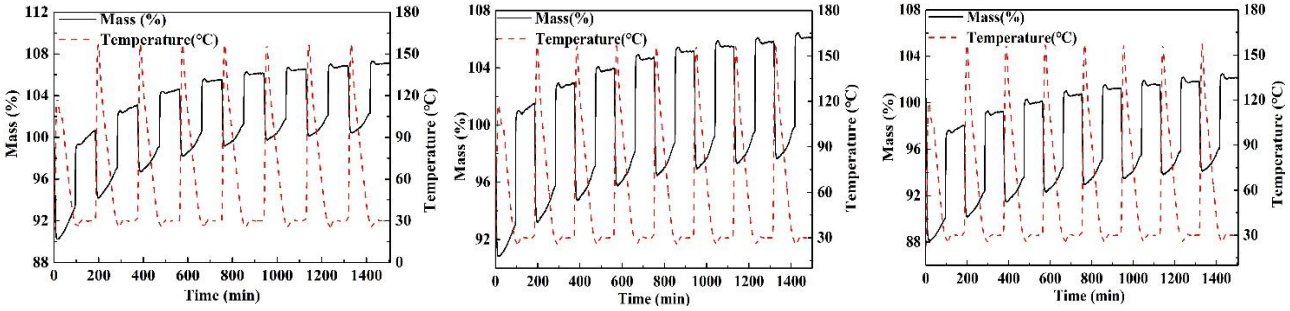

(a) N_2-600J (b) N_2-800J (c) N_2-1000J

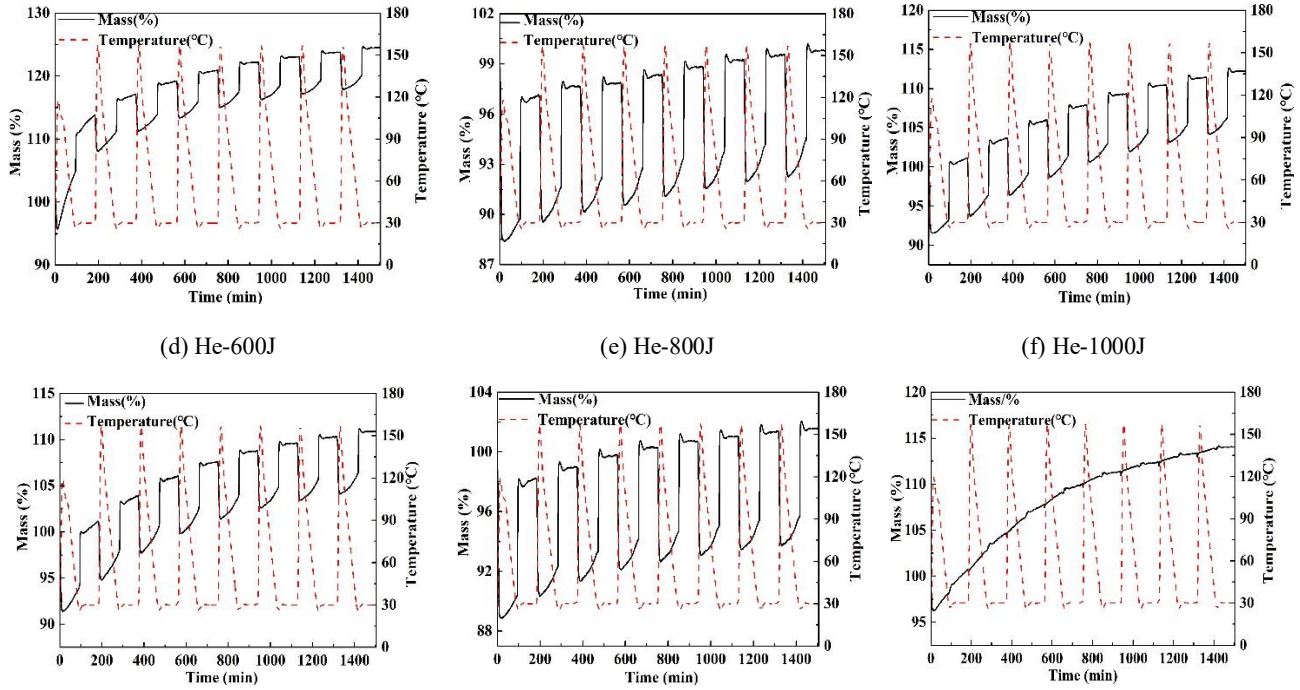

(d) He-600J (e) He-800J (f) He-1000J

(g) CO_2-600J (h) CO_2-800J (i) CO_2-1000J

Fig. 4 CO_2 multiple adsorption curves of MG chars at 140 °C desorption temperature: (a)-(c) N_2 atmosphere, (d)-(f) He atmosphere and (g)-(i) CO_2 atmosphere.

The comparison of the CO_2 adsorption capacity of different MG chars is shown in Fig. 5. The CO_2 adsorption capacity of MG chars decreased with the increasing number of the adsorption/desorption cycles. According to the observation and comparison of adsorption capacity and loss rate of the adsorption capacity of MG chars regenerated at 140 °C, it was found that the performance of MG chars was stablised after four adsorption/desorption cycles. The adsorption capacity of cyclic adsorption was related to the regeneration degree of an adsorbent. The more complete the regeneration desorption was, the higher the repeated adsorption capacity was, and vice versa. After four cycles of regeneration, the adsorption capacity of He-600J was the lowest, dropped from 1.483 to 1.042 mmol·g^{-1}, and the loss rate reached 27.58%. However, after seven cycles of regeneration, the regeneration ability of CO_2-1000J was the lowest, dropped from 0.208 to 0.052 mmol·g^{-1}. The loss rate of adsorption capacity was as high as 75%. The cyclic regeneration adsorption capacity of N_2-600J, He-600J and CO_2-600J were the lowest, comparing to the values of MG chars prepared at higher temperatures under the same atmosphere (except CO_2-1000J). The three samples had the highest loss rate of the adsorption capacity. After the fourth adsorption-desorption cycles, the loss rate was higher than 24%, and after the seventh cycles, the loss rate was higher than 30%. This was because that the MG chars prepared at 600 °C was rich in amino [42] and hydroxyl [43] groups, and reactions between the functional groups and CO_2 that occurred during adsorption caused their deactivation. When the char production temperature was 800 °C, as compared with 600 °C, the cyclic adsorption capacity of MG chars prepared in the same atmosphere increased, and the cyclic adsorption loss rate decreased. This was due to the synergistic effect of physical adsorption and chemical adsorption on the cyclic adsorption performance of MG chars. Although the amino and hydroxyl groups on the surface of MG chars were reduced, causing less chemical adsorption of CO_2, but the pore structure of MG chars was extended so that the physical adsorption increased. The adsorption capacity of N_2-800J was 1.405 mmol·g^{-1}, and

the loss rate was only 22.78% after seven times cyclic regeneration. Therefore, the char N_2-800J had the best cyclic regeneration adsorption performance.

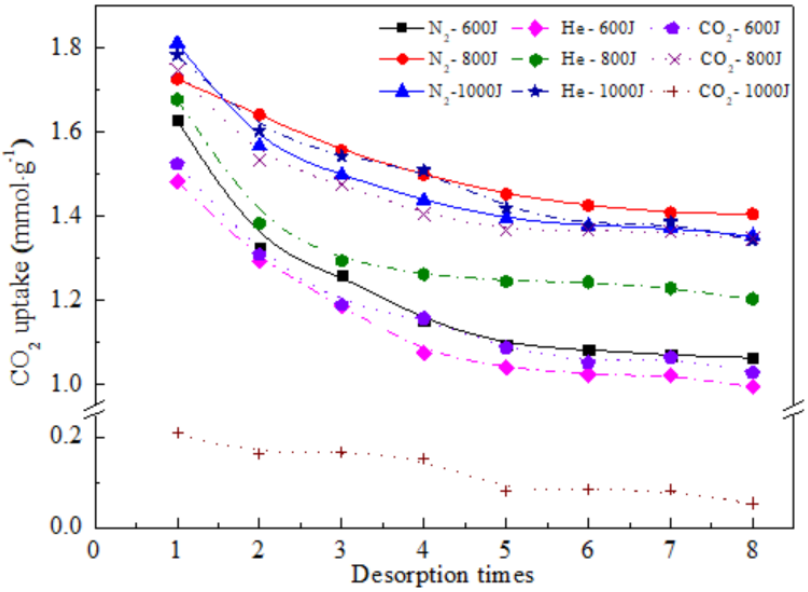

Fig. 5 CO_2 capacity of cyclic adsorption of MG char at desorption temperature of 140 °C.

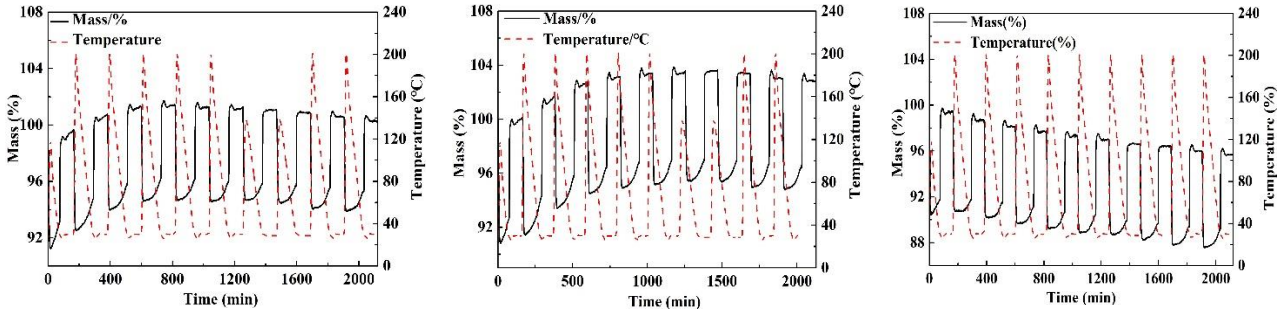

(a) N_2-600J (b) N_2-800J (c) N_2-1000J

Fig. 6 CO_2 cyclic adsorption curves of N_2 char prepared at (a)600 °C, (b)800 °C and (c)1000 °C (at the desorption temperature of 180 °C).

To study the influence of the desorption temperature on the adsorption capacity and cyclic regeneration adsorption performance of samples, MG chars prepared under N_2 atmosphere were selected for seven CO_2 cyclic regeneration measurements at the desorption temperature of 180 °C. Fig. 6 shows the CO_2 cyclic regeneration adsorption curve of N_2-600J, N_2-800J and N_2-1000J at the desorption temperature of 180 °C. And the raw CO_2 cyclic adsorption capacity (mmol·g^{-1}) and adsorption loss rate of MG chars desorption at 180 °C are shown in Table 3.

Table 3 CO_2 cyclic adsorption capacity (mmol·g^{-1}) at 30 °C and adsorption loss rate of MG char desorption at 180 °C.

Samples	1	2	3	4	5	6	7	8	1-Loss [a] (%)	4-Loss [b] (%)	7-Loss [c] (%)
N_2-600J	1.485	1.359	1.264	1.187	1.158	1.185	1.188	1.163	8.49	22.02	27.69
N_2-800J	1.684	1.669	1.575	1.520	1.501	1.494	1.506	1.479	0.891	10.87	13.86
N_2-1000J	1.741	1.575	1.520	1.499	1.496	1.490	1.501	1.488	9.53	14.07	17.00

[a] Adsorption loss rate of MG after desorption for one time. [b] Adsorption loss rate of MG after desorption for four times. [c] Adsorption loss

rate of MG after desorption for seven times.

It can be seen from Fig. 6 and Table 3 that when the desorption temperature was 180 °C, the cyclic regeneration performance of each sample was better than that regenerated at 140 °C (Table 2). The first, fourth and seventh adsorption capacity loss rates of N_2-600J decreased from 13.42, 24.61 and 30.43 % at 140 °C to 8.49, 22.02 and 27.69 % at 180 °C, respectively. When the desorption temperature was 180 °C, the cyclic regeneration efficiency of N_2-800J was the highest, the adsorption loss rate of a single cycle was only 0.891 %, and the adsorption loss rate of 4 and 7 cycles was 10.87 and 13.86 %, respectively. This was because the higher desorption temperature increased the desorption degree of CO_2 adsorbed on MG chars, which decreased the loss rate of adsorption capacity in the cyclic adsorption on MG chars.

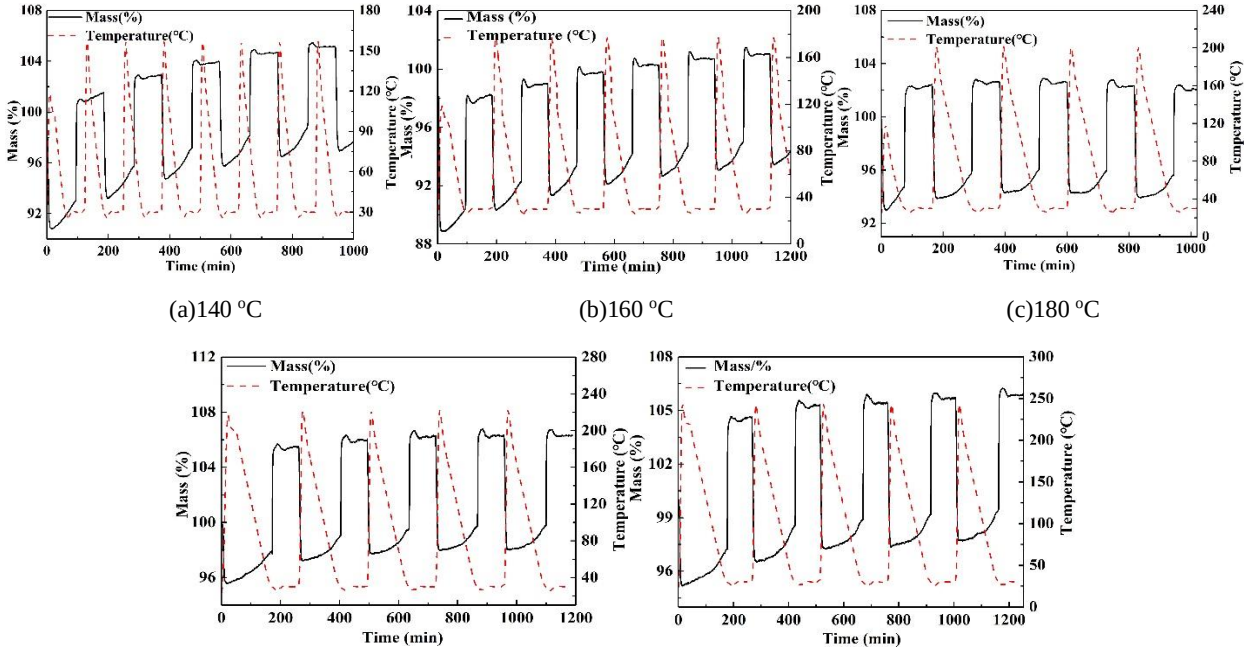

(a)140 °C (b)160 °C (c)180 °C

(d)200 °C (e)220 °C

Fig. 7 CO_2 Cyclic adsorption curves of N_2-800J at at the desorption temperature of (a)140 °C, (b)160 °C, (c)180 °C, (d)200 °C and (e)220 °C.

It can be seen from the literature [46] that the cyclic regeneration efficiency of samples varies greatly with the change in the desorption temperature. In order to verify that N_2-800J had the highest regeneration efficiency at 180 °C, N_2-800J was then regenerated four times at 160, 200 and 220 °C respectively. The adsorption cycle, adsorption capacity and CO_2 multiple adsorption curves of active regeneration are shown in Fig. 7. Table 4 shows the adsorption capacity of active regeneration of N_2-800J at 140, 160, 180 200 and 220 °C.

Table 4 CO_2 cyclic adsorption capacity (mmol·g^{-1}) and adsorption loss rate of MG char at different desorption temperatures.

Temperatures	1	2	3	4	5	1-Loss [a] (%)	4-Loss [b] (%)
140 °C	1.725	1.641	1.555	1.498	1.452	4.87	15.83
160 °C	1.657	1.594	1.506	1.455	1.453	3.80	12.31
180 °C	1.684	1.669	1.575	1.520	1.501	0.89	10.87

200 °C	1.716	1.571	1.545	1.490	1.494	8.45	12.94
220 °C	1.640	1.510	1.483	1.461	1.447	7.93	11.77

[a] Adsorption loss rate of MG after desorption for one time. [b] Adsorption loss rate of MG after desorption for four times.

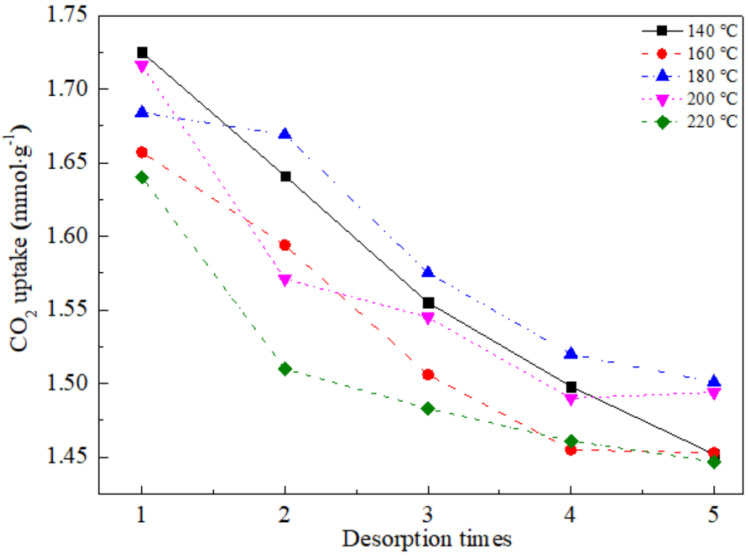

Fig. 8 Cyclic adsorption capacity of N_2-800J at different desorption temperatures.

By comparing the loss rate of the cyclic regeneration adsorption capacity of N_2-800J at different temperatures in Table 4, it could be confirmed that N_2-800J had the lowest loss rate when the desorption temperature was 180 °C. The cyclic regeneration adsorption capacities of N_2-800J at different desorption temperatures are shown in Fig. 8. The adsorption capacity of CO_2 obtained after desorption at 140 °C was higher than those at other desorption temperatures, indicating that at 140 °C, the sample had not yet achieved complete desorption, and some CO_2 molecules were still adsorbed on the char sample. When the desorption temperature increased to 160 °C, the loss rate of cyclic adsorption capacity reduced, indicating that the degree of desorption increased. However, the adsorption capacity at 160 °C was lower than that at 140 °C, which might be due to the stable semicarbazide formed by the dehydration reaction between CO_2 and the amino group on the surface of MG chars over 135 °C, causing the deactivation of the sample [42]. At the same time, the higher the desorption temperature was, the stronger reaction of hydroxyl with CO_2 was, which might be another reason for the deactivation of MG chars. With the further increase of desorption temperature, the adsorption capacity of N_2-800J was improved at 180 °C with the lowest loss rate of 10.87%. When the temperature continued to rise to above 200 °C, the cyclic adsorption capacity of the sample decreased. It might be caused by partial decomposition at high temperature or enhanced reaction with CO_2. According to the experimental findings, the best desorption temperature was 180 °C.

4. Conclusions

In this paper, the CO_2 adsorption and recycling properties of MG chars were studied by thermogravimetry. The effects of char production atmosphere, char production temperature and desorption temperature on the CO_2 adsorption capacity of the MG chars were analysed. The effects of the physic-chemical properties of the MG chars on the CO_2 adsorption and recycling properties were investigated. The conclusions are as follows:

(1) Based on the study of the physical and chemical characteristics and CO_2 uptake experiment on MG chars, it was found that the microcrystalline structure, micropore size, chemical characteristics, and desorption temperature of MG chars were the main factors affecting the adsorption and desorption of CO_2.

(2) Based on the study of char production atmosphere, char production temperature and desorption temperature, it was found that the char production atmosphere and char production temperature together affected the physic-chemical properties of the MG chars, thus affected the adsorption capacity of the MG chars for CO_2 at 30 ^oC. The most excellent single adsorption performance was N_2-1000J (with a CO_2 capacity of 1.811 $mmol \cdot g^{-1}$). When the desorption temperature was 140 ^oC, after seven cycles of regeneration, it was found that the loss rate of the CO_2 adsorption capacity of N_2-800J was the lowest (ca. 22.78%).

(3) It was found that the best desorption temperature was 180 ^oC. After cyclic regeneration adsorption four times, the CO_2 adsorption loss rate at the desorption temperature of 180 ^oC was the lowest (ca. 10.87%) compared to other desorption temperatures.

(4) The results of this study confirmed that the MG chars were suitable adsorbents for CO_2 capture. Physical adsorption and chemical adsorption coexisted during the CO_2 adsorption on MG chars.

Declaration of Competing Interest

The authors declare that they have no known competing financial interests or personal relationships that could have appeared to influence the work reported in this paper.

Acknowledgements

This project was supported by the Natural Science Foundation of China for Young Scholars (No.51706022), the Natural Science Foundation of Hunan Province of China (No. 2019JJ40299), the Education Department Foundation of Hunan Province of China (No. 20A004, No. 20B041) and the Innovative Team of Key Technologies of Energy Conservation, Emission Reduction and Intelligent Control for Power-Generating Equipment and System at CSUST. This project has received funding from the European Union's Horizon 2020 research and innovation programme under the Marie Skłodowska-Curie grant agreement (GreenCarbon No. 721991). The work was also supported by an Institutional Links grant (No. 527641843), under the Turkey partnership. The grant is funded by the UK Department for Business, Energy and Industrial Strategy and delivered by the British Council.

CRediT authorship contribution statement

Hong Tian: Conceptualization, Methodology, Investigation, Writing - original draft. **Tong Zhou:** Methodology, Investigation, Formal analysis, Data curation, Writing - original draft. **Jiawei Wang:** Writing - review & editing, Funding acquisition. **Filipe Rego:** Investigation, Formal analysis. **Yang Yang:** Supervision, Funding acquisition. **Huan Xiang:** Data validation, Writing - review & editing. **Yanshan Yin:** Data validation, Data curation. **Wei Liu:** Data curation, Investigation. **Anthony V. Bridgwater:** Supervision, Funding acquisition.

References

[1] N. Shehzad, M. Tahir, K. Johari, T. Murugesan, M. Hussain, A critical review on TiO_2 based photocatalytic CO_2 reduction system: Strategies to improve efficiency, J. CO_2 Util. 26 (2018) 98-122, https://doi.org/10.1016/j.jcou.2018.04.026.

[2] B. Zhu, C. Shang, Z. Guo, Naturally Nitrogen and Calcium-Doped Nanoporous Carbon from Pine Cone with Superior CO_2 Capture Capacities, ACS Sustain. Chem. Eng. 4 (2016) 1050-1057, https://doi.org/10.1021/acssuschemeng.5b01113.

[3] T.A. Atsbha, T. Yoon, P. Seongho, C.-J. Lee, A review on the catalytic conversion of CO_2 using H_2 for synthesis of CO, methanol, and hydrocarbons, J. CO_2 Util. 44 (2021) 101413, https://doi.org/10.1016/j.jcou.2020.101413.

[4] S. Zhang, N. Gao, F. Wang, C. Wu, Autothermal CaO looping biomass gasification to increase process energy efficiency and reduce ash sintering, Fuel 277 (2020) 118199, https://doi.org/10.1016/j.fuel.2020.118199.

[5] N. Hsan, P.K. Dutta, S. Kumar, N. Das, J. Koh, Capture and chemical fixation of carbon dioxide by chitosan grafted multi-walled carbon nanotubes, J. CO_2 Util. 41 (2020) 101237, https://doi.org/10.1016/j.jcou.2020.101237.

[6] C. Shi, L. Li, Y. Li, High-throughput screening of hypothetical aluminosilicate zeolites for CO_2 capture from flue gas, J. CO_2 Util. 42 (2020) 101346, https://doi.org/10.1016/j.jcou.2020.101346.

[7] D.K. Yoo, N. Abedin Khan, S.H. Jhung, Polyaniline-loaded metal-organic framework MIL-101(Cr): Promising adsorbent for CO_2 capture with increased capacity and selectivity by polyaniline introduction, J. CO_2 Util. 28 (2018) 319-325, https://doi.org/10.1016/j.jcou.2018.10.012.

[8] M. Liu, M.D. Nothling, P.A. Webley, J. Jin, Q. Fu, G.G. Qiao, High-throughput CO_2 capture using PIM-1@MOF based thin film composite membranes, Chem. Eng. J. 396 (2020) 125328, https://doi.org/10.1016/j.cej.2020.125328.

[9] H. Sun, W. Gao, Y. Zhang, X. Cao, S. Bao, P. Li, et al., Bis(phenyl)fluorene-based polymer of intrinsic microporosity/functionalized multi-walled carbon nanotubes mixed matrix membranes for enhanced CO_2 separation performance, React. Funct. Polym. 147 (2020) 104465, https://doi.org/10.1016/j.reactfunctpolym.2019.104465.

[10] Y. Sang, L. Shao, J. Huang, Carbonyl functionalized hyper-cross-linked polymers for CO_2 capture, J. Polym. Res. 27 (2020) 188-196, https://doi.org/10.1007/s10965-020-02146-w.

[11] H.R. Penchah, A. Ghaemi, H.G. Gilani, Benzene-Based Hyper-Cross-Linked Polymer with Enhanced Adsorption Capacity for CO_2 Capture, Energy Fuels 33 (2019) 12578-12586, https://doi.org/10.1021/acs.energyfuels.9b03136.

[12] V.S.P.K. Neti, J. Wang, S. Deng, L. Echegoyen, Selective CO_2 adsorption in a porphyrin polymer with benzimidazole linkages, RSC Adv. 5 (2015) 10960-10963, https://doi.org/10.1039/c4ra15086d.

[13] V.S.P.K. Neti, J. Wang, S. Deng, L. Echegoyen, High and selective CO_2 adsorption by a phthalocyanine nanoporous polymer, J. Mater. Chem. A 3 (2015) 10284-10288, https://doi.org/10.1039/c5ta00587f.

[14] V. Zelenak, M. Skrinska, F.R. Siperstein, A. Patti, Phase evolution during one-pot synthesis of amine modified mesoporous silica materials: Preparation, properties, carbon dioxide adsorption, Appl. Surf. Sci. 476 (2019) 886-896, https://doi.org/10.1016/j.apsusc.2019.01.146.

[15] N. Gao, M. Śliz, C. Quan, A. Bieniek, A. Magdziarz, Biomass CO_2 gasification with CaO looping for syngas production in a fixed-bed reactor, Renew. Energy 167 (2021) 652-661, https://doi.org/10.1016/j.renene.2020.11.134.

[16] N. Gao, K. Chen ,C. Quan, Development of CaO-based adsorbents loaded on charcoal for CO_2 capture at high temperature, Fuel 260 (2020) 116411, https://doi.org/10.1016/j.fuel.2019.116411.

[17] T. Khandaker, M.S. Hossain, P.K. Dhar, M.S. Rahman, M.A. Hossain, M.B. Ahmed, Efficacies of Carbon-Based Adsorbents for Carbon Dioxide Capture, Processes 8 (2020) 654, https://doi.org/10.3390/pr8060654.

[18] J. Wang, R. Krishna, J. Yang, K.P.R. Dandamudi, S. Deng, Nitrogen-doped porous carbons for highly selective CO_2 capture from flue gases and natural gas upgrading, Mater. Today Commun. 4 (2015) 156-165, https://doi.org/10.1016/j.mtcomm.2015.06.009.

[19] V. Gargiulo, A. Gomis-Berenguer, P. Giudicianni, C.O. Ania, R. Ragucci, M. Alfe, Assessing the Potential of Biochars Prepared by Steam-Assisted Slow Pyrolysis for CO_2 Adsorption and Separation, Energy Fuels 32 (2018) 10218-10227, https://doi.org/10.1021/acs.energyfuels.8b01058.

[20] J. Yang, L. Yue, X. Hu, L. Wang, Y. Zhao, Y. Lin, et al., Efficient CO_2 Capture by Porous Carbons Derived from Coconut Shell, Energy Fuels 31 (2017) 4287-4293, https://doi.org/10.1021/acs.energyfuels.7b00633.

[21] A. Heidari, H. Younesi, A. Rashidi, A.A. Ghoreyshi, Evaluation of CO_2 adsorption with eucalyptus wood based activated carbon modified by ammonia solution through heat treatment, Chem. Eng. J. 254 (2014) 503-513, https://doi.org/10.1016/j.cej.2014.06.004.

[22] S. Shahkarami, A.K. Dalai, J. Soltan, Y. Hu, D. Wang, Selective CO_2 Capture by Activated Carbons: Evaluation of the Effects of Precursors and Pyrolysis Process, Energy Fuels 29 (2015) 7433-7440, https://doi.org/10.1021/acs.energyfuels.5b00470.

[23] A.E. Creamer, B. Gao, M. Zhang, Carbon dioxide capture using biochar produced from sugarcane bagasse and hickory wood, Chem. Eng. J. 249 (2014) 174-179, https://doi.org/10.1016/j.cej.2014.03.105.

[24] H. Madzaki, W.A.W.A.B. KarimGhani, NurZalikhaRebitanim, AzilBahariAlias, Carbon Dioxide Adsorption on Sawdust Biochar, Procedia Eng. 148 (2016) 718-725, https://doi.org/10.1016/j.proeng.2016.06.591.

[25] Y.-F. Huang, P.-T. Chiueh, C.-H. Shih, S.-L. Lo, L. Sun, Y. Zhong, et al., Microwave pyrolysis of rice straw to produce biochar as an adsorbent for CO_2 capture, Energy 84 (2015) 75-82, https://doi.org/10.1016/j.energy.2015.02.026.

[26] H. Zhuo, Y. Hu, X. Tong, L. Zhong, X. Peng, R. Sun, Sustainable hierarchical porous carbon aerogel from cellulose for high-performance supercapacitor and CO_2 capture, Ind. Crops Prod. 87 (2016) 229-235, https://doi.org/10.1016/j.indcrop.2016.04.041.

[27] Y.-J. Heo, S.-J. Park, A role of steam activation on CO_2 capture and separation of narrow microporous carbons produced from cellulose fibers, Energy 91 (2015) 142-150, https://doi.org/10.1016/j.energy.2015.08.033.

[28] M.G. Plaza, A.S. Gonzalez, J.J. Pis, F. Rubiera, C. Pevida, Production of microporous biochars by single-step oxidation: Effect of activation conditions on CO_2 capture, Appl. Energy 114 (2014) 551-562, https://doi.org/10.1016/j.apenergy.2013.09.058.

[29] F. Shen, Y. Wang, L. Li, K. Zhang, R.L. Smith, X. Qi, Porous carbonaceous materials from hydrothermal carbonization and KOH activation of corn stover for highly efficient CO_2 capture, Chem. Eng. Commun. 205 (2018) 423-431, https://doi.org/10.1080/00986445.2017.1367671.

[30] J.J. Manya, B. Gonzalez, M. Azuara, G. Arner, Ultra-microporous adsorbents prepared from vine shoots-derived biochar with high CO_2 uptake and CO_2/N_2 selectivity, Chem. Eng. J. 345 (2018) 631-639, https://doi.org/10.1016/j.cej.2018.01.092.

[31] M.G. Plaza, S. Garcia, F. Rubiera, J.J. Pis, C. Pevida, Evaluation of ammonia modified and conventionally activated biomass based carbons as CO_2 adsorbents in postcombustion conditions, Sep. Purif. Technol. 80 (2011) 96-104, https://doi.org/10.1016/j.seppur.2011.04.015.

[32] N. Alvarez-Gutierrez, M.V. Gil, F. Rubiera, C. Pevida, Adsorption performance indicators for the CO_2/CH_4 separation: Application to biomass-based activated carbons, Fuel Process. Technol. 142 (2016) 361-369, https://doi.org/10.1016/j.fuproc.2015.10.038.

[33] J. Chen, J. Yang, G. Hu, X. Hu, Z. Li, S. Shen, et al., Enhanced CO_2 Capture Capacity of Nitrogen-Doped Biomass-Derived Porous Carbons, ACS Sustain. Chem. Eng. 4 (2016) 1439-1445, https://doi.org/10.1021/acssuschemeng.5b01425.

[34] H. Tian, Q.S. Hu, J.W. Wang, L. Liu, Y. Yang, A.V. Bridgwater, Steam gasification of Miscanthus derived char: the reaction kinetics and reactivity with correlation to the material composition and microstructure, Energy Convers. Manage. 219 (2020) 113026, https://doi.org/10.1016/j.enconman.2020.113026.

[35] H. Tian, Q. Hu, J. Wang, D. Chen, Y. Yang, A.V. Bridgwater, Kinetic study on the CO_2 gasification of biochar derived from Miscanthus at different processing conditions, Energy 217 (2021) 119341, https://doi.org/10.1016/j.energy.2020.119341.

[36] J. Wang, L.A. Stevens, T.C. Drage, J. Wood, Preparation and CO_2 adsorption of amine modified Mg–Al LDH via exfoliation route, Chem. Eng. Sci. 68 (2012) 424-431, https://doi.org/10.1016/j.ces.2011.09.052.

[37] E.M. Calvo-Munoz, F.J. Garcia-Mateos, J.M. Rosas, J. Rodriguez-Mirasol, T. Cordero, Biomass Waste Carbon Materials as adsorbents for CO_2 Capture under Post-Combustion Conditions, Front. Mater. 3 (2016) 23, https://doi.org/10.3389/fmats.2016.00023.

[38] C. Quan, X. Jia, N. Gao, Nitrogen-doping activated biomass carbon from tea seed shell for CO_2 capture and supercapacitor, Int. J. Energy Res. 44 (2019) 1218-1232, https://doi.org/10.1002/er.5017.

[39] C. Quan, R. Su, N. Gao, Preparation of activated biomass carbon from pine sawdust for supercapacitor and CO_2 capture, Int. J. Energy Res. 44 (2020) 4335-4351, https://doi.org/10.1002/er.5206.

[40] S.M. Hong, E. Jang, A.D. Dysart, V.G. Pol, K.B. Lee, CO_2 Capture in the Sustainable Wheat-Derived Activated Microporous Carbon Compartments, Sci. Rep. 6 (2016) 34590, https://doi.org/10.1038/srep34590.

[41] B. Zhao, J. Wang, D. Zhu, G. Song, H. Yang, L. Chen, et al., Adsorption Characteristics of Gas Molecules (H_2O, CO_2, CO, CH_4, and H_2) on CaO-Based Catalysts during Biomass Thermal Conversion with in Situ CO_2 Capture, Catalysts 9 (2019) 757, https://doi.org/10.3390/catal9090757.

[42] T.C. Drage, A. Arenillas, K.M. Smith, C.E. Snape, Thermal stability of polyethylenimine based carbon dioxide adsorbents and its influence on selection of regeneration strategies, Microporous Mesoporous Mater. 116 (2008) 504-512, https://doi.org/10.1016/j.micromeso.2008.05.009.

[43] G. Singh, K.S. Lakhi, S. Sil, S.V. Bhosale, I. Kim, K. Albahily, et al., Biomass derived porous carbon for CO_2 capture, Carbon 148 (2019) 164-186, https://doi.org/10.1016/j.carbon.2019.03.050.

[44] C. Quan, H. Wang, X. Jia, N. Gao, Effect of carbonization temperature on CO_2 adsorption behavior of activated coal char, J. Energy Inst. 97 (2021) 92-99, https://doi.org/10.1016/j.joei.2021.04.003.
[45] I. Duran, F. Rubiera, C. Pevida, Separation of CO_2 in a Solid Waste Management Incineration Facility Using Activated Carbon Derived from Pine Sawdust, Energies 10 (2017) 827, https://doi.org/10.3390/en10060827.
[46] C. Zhao, Y. Guo, J. Yan, J. Sun, W. Li, P. Lu, Enhanced CO_2 sorption capacity of amine-tethered fly ash residues derived from co-firing of coal and biomass blends, Appl. Energy 242 (2019) 453-461, https://doi.org/10.1016/j.apenergy.2019.03.143.